THE JOURNAL OF PHYSICAL CHEMISTRY B
A JOURNAL OF THE AMERICAN CHEMICAL SOCIETY

pubs.acs.org/JPCB

Article

Surface Properties of *N,N*-Dimethylformamide–Water Mixtures, As Seen from Computer Simulations

Barbara Honti, Balázs Fábián, Abdenacer Idrissi, and Pál Jedlovszky*

Cite This: *J. Phys. Chem. B* 2023, 127, 1050–1062

Read Online

ACCESS | Metrics & More | Article Recommendations

ABSTRACT: The liquid–vapor interface of *N,N*-dimethylformamide (DMF)–water mixtures, spanning the entire composition range, is investigated in detail at 298 K by molecular dynamics simulation and intrinsic surface analysis. DMF molecules are found to adsorb strongly at the liquid surface, but this adsorption extends only to the first molecular layer. Water and DMF molecules mix with each other on the molecular scale even in the surface layer; thus, no marked self-association of any of the components is seen at the liquid surface. The major surface component prefers such orientation in which the molecular dipole vector lays parallel with the macroscopic plane of the surface. On the other hand, the preferred orientation of the minor component is determined, at both ends of the composition range, by the possibility of H-bond formation with the major component. The lack of H-donating ability of DMF leads to a rapid breakup of the percolating H-bond network at the surface; due to the strong adsorption of DMF, this breakup occurs below the bulk phase DMF mole fraction of 0.03. The disruption of the surface H-bond network also accelerates the exchange of both species between the liquid surface and bulk liquid phase, although, for water, this effect becomes apparent only above a bulk phase DMF mole fraction of 0.4. H-bonds formed by a DMF and a water molecule live, on average, 25–60% longer than those formed by two water molecules at the liquid surface. A similar, but smaller (i.e., about 10–20%) difference is seen in the bulk liquid phase. The enhanced surface mobility of the molecules results in 2–6 times larger diffusion coefficient and 2–5 times shorter H-bond lifetime values at the liquid surface than in the bulk liquid phase. The diffusion of both molecules is slowed down in the presence of the other species; in the case of DMF, this effect is caused by the formation of water–DMF H-bonds, whereas for water, steric hindrances imposed by the bulky DMF neighbors are responsible for this slowing down.

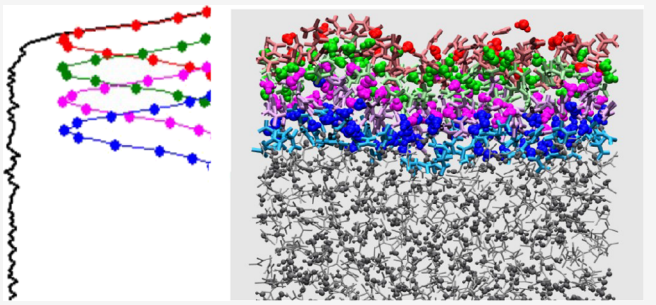

1. INTRODUCTION

N,N-Dimethylformamide (DMF) and its aqueous mixtures are among the most widely used organic solvents. The excellent solvation abilities of such systems are related to the molecular structure of DMF. Thus, although the DMF molecule is strongly polar (its dipole moment being as large as 3.9 D),[1] it is one of the smallest amphiphiles, as it also bears two apolar CH_3 groups. Further, although the O atom of the DMF molecule is able to accept H-bonds, the lack of donable H atoms makes neat DMF an aprotic solvent (although the CH_3 hydrogens are thought to participate in weak, C–H···O type H-bonds[2,3]). This fact is also reflected in a rather low dielectric constant value of DMF of about 40.[4] However, adding water to DMF immediately turns on the H-bond formation,[3] which makes DMF–water mixtures highly non-ideal.[5,6] This non-ideal behavior is in a clear contrast with that of aqueous mixtures of formamide, i.e., the double demethylated analogue of DMF, which is regarded to be nearly ideal.[7−10] Thus, the properties of aqueous DMF mixtures are governed by the delicate interplay of hydrophobic, dipolar, and H-bonding interactions. Furthermore, DMF is the smallest aprotic molecule that bears a peptide bond, enabling its aqueous solutions to be used as biomimetic models of hydrated proteins.[11−13]

The aforementioned delicate interplay of various interactions makes aqueous DMF mixtures suitable solvents in various purposes. Indeed, these mixtures are widely used in a number of fields both in chemistry and in the chemical industry. The areas of chemical and industrial applications include electrospinning,[14−18] electrochemistry,[19−21] synthesis of various nanoparticles[18,22−24] and organic molecules,[25−32] including microwave-enhanced reactions,[29−32] hydrolysis of highly charged metal ions,[33] as well as cellulosic biomass processing,[34] and the production of, among others, adhesives,

Received: October 28, 2022
Revised: December 12, 2022
Published: January 18, 2023

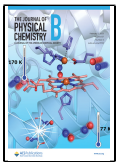

https://doi.org/10.1021/acs.jpcb.2c07572
J. Phys. Chem. B 2023, 127, 1050–1062

Table 1. Characteristics of the Systems Simulated[a]

						τ_{HB}/ps		τ_{surf}/ps		τ_D/ps		$D_{\parallel}$/Å^{2}ps^{-1}	
N_{DMF}	N_{wat}	x_{DMF}	x^b_{DMF}	x^1_{DMF}	γ/mN m^{-1}	water−water	water−DMF	DMF	water	DMF	water	DMF	water
0	4000	0	0	0	65.1 ± 0.5	1.45 (*2.86*)			12.0		6.37		0.48 (*0.20*)
200	3800	0.05	0.03	0.28	52.4 ± 0.6	1.40 (*3.42*)	1.77 (*3.81*)	233	8.9	32.3	9.20	0.21 (*0.074*)	0.33 (*0.15*)
400	3600	0.1	0.08	0.37	48.1 ± 0.6	1.41 (*4.01*)	1.82 (*4.61*)	176	9.2	36.6	11.0	0.19 (*0.061*)	0.28 (*0.11*)
800	3200	0.2	0.19	0.50	47.8 ± 0.8	1.45 (*5.10*)	1.94 (*5.87*)	151	10.0	38.5	10.0	0.18 (*0.049*)	0.30 (*0.078*)
1200	2800	0.3	0.29	0.60	43.4 ± 1.1	1.51 (*6.12*)	2.27 (*7.03*)	127	10.2	38.8	8.67	0.18 (*0.047*)	0.35 (*0.063*)
1600	2400	0.4	0.40	0.67	44.5 ± 1.0	1.58 (*7.05*)	2.07 (*8.29*)	112	10.6	36.4	8.99	0.19 (*0.047*)	0.34 (*0.056*)
2000	2000	0.5	0.49	0.76	42.8 ± 0.6	1.29 (*8.37*)	2.12 (*9.41*)	89.7	9.9	29.6	8.17	0.23 (*0.053*)	0.37 (*0.056*)
2400	1600	0.6	0.60	0.83	41.6 ± 1.4	1.32 (*8.49*)	2.16 (*10.3*)	73.6	9.1	24.3	6.40	0.28 (*0.069*)	0.47 (*0.068*)
2800	1200	0.7	0.71	0.88	39.6 ± 1.0	1.28 (*8.94*)	2.07 (*11.2*)	62.2	8.1	21.0	6.53	0.33 (*0.088*)	0.46 (*0.086*)
3200	800	0.8	0.79	0.93	38.7 ± 0.4	0.97 (*8.27*)	2.15 (*11.6*)	53.5	7.5	17.6	5.07	0.39 (*0.11*)	0.59 (*0.11*)
3600	400	0.9	0.90	0.97	38.0 ± 1.1	1.19 (*9.36*)	2.03 (*11.3*)	47.7	6.9	15.7	5.89	0.44 (*0.13*)	0.51 (*0.13*)
3800	200	0.95	0.95	0.98	37.8 ± 0.5	0.70 (*9.23*)	1.55 (*10.1*)	45.4	6.2	14.4	5.46	0.48 (*0.14*)	0.55 (*0.14*))
4000	0	1	1	1	36.4 ± 1.2			43.8		13.9		0.49 (*0.14*)	

[a]Italic values in parentheses refer to the bulk liquid phase.

fibers, pesticides, plastics, and synthetic leathers.[35] Many of these applications involve, besides the bulk liquid phase, also the surface of DMF−water mixtures. However, while the bulk phase properties of water−DMF mixtures have been thoroughly investigated in the past few decades,[2−6,36−48] investigations of the surface of such mixtures are scarce. In fact, we are only aware of one such study, in which the surfaces of aqueous DMF mixtures of various compositions were investigated by sum frequency generation spectroscopy, revealing that DMF induces randomness in the surface orientation of water molecules.[49]

Experimental investigations can be well complemented by computer simulation studies, as simulations can provide such a deep, molecular level insight into a suitably chosen model of the system that cannot be obtained from experiments.[50] However, it should be emphasized that computer simulations treat a model instead of the system of interest itself, and hence, the choice of the model needs to be validated by comparing simulation results with as many experimental data as possible.[50] To study liquid DMF, a number of potential models were developed in the past few decades.[1,6,51−55] However, when investigating binary mixtures, the ability of the models to reproduce the properties of the two neat liquids is a necessary but not sufficient condition of reliably simulating also their mixtures.[56,57] For this reason, we have recently developed a new model of DMF, referred to as HIJ,[6] by optimizing its mixing properties with the TIP4P/2005[58] water model.

In this paper, we present a detailed analysis of the structural and dynamical properties of the liquid−vapor interface of DMF−water mixtures of various compositions by molecular dynamics simulations. In the simulations, the aforementioned HIJ[6] and TIP4P/2005[58] models of DMF and water, respectively, have been used, as this model combination was shown to well reproduce a number of properties of not only the two neat liquids but also of their mixtures.[6] To identify the real, capillary wave corrugated, molecularly rough surface of the liquid phase, we have used the identification of the truly interfacial molecules (ITIM) method,[59] representing an excellent compromise between computational cost and accuracy.[60] The properties investigated include the arrangement of the molecules both in the macroscopic plane of the interface and along its normal, adsorption of DMF in the subsequent molecular layers at the liquid surface, and H-bonding, orientation, residence time, and diffusion of the DMF and water molecules within the surface layer.

The paper is organized as follows. In Section 2, details of the calculations, including molecular dynamics simulations and ITIM analyses, are given. The obtained results concerning both the structure and dynamics of the liquid surface are detailed and discussed in Section 3. Finally, in Section 4, the main conclusions of this study are summarized.

2. METHODS

2.1. Molecular Dynamics Simulations. The liquid−vapor interfaces of DMF−water mixtures of 11 different compositions have been simulated by molecular dynamics in the canonical (N,V,T) ensemble at a temperature of 298 K. The mole fraction of DMF, x_{DMF}, has been 0.05, 0.1, 0.2, 0.3, 0.4, 0.5, 0.6, 0.7, 0.8, 0.9, and 0.95 in these systems. In addition, simulations of the two neat systems have also been performed for reference purposes. All systems have consisted of 4000 molecules. The number of DMF and water molecules present in the basic box (N_{DMF} and N_{wat}, respectively) in the different systems is collected in Table 1. The lengths of the X, Y, and Z edges of the rectangular basic box have been 300, 50, and 50 Å, respectively, X being the macroscopic surface normal axis.

DMF and water molecules have been described by the HIJ[6] and TIP4P/2005[58] potential models, respectively, as this model combination has recently been shown to excellently reproduce, besides those of the two neat liquids, also the properties of their mixtures.[6] Both of these models are pairwise additive; thus, the total potential energy of the system is estimated to be the sum of the interaction energies of all molecule pairs, while the interaction energy of a given pair of molecules is the sum of the Lennard-Jones and charge−charge Coulomb contributions of all pairs of their interaction sites. The HIJ model treats the methyl groups of the DMF molecule as united atoms,[6] while the TIP4P/2005 model bears an additional, non-atomic interaction site, denoted as M, along the bisector of the H−O−H bond angle.[58] The Lennard-Jones energy and distance parameters (ε and σ, respectively) and fractional charges (q) of the interaction sites of the two models are collected in Table 2. The Lennard-Jones parameters of unlike atom pairs have been combined according to the Lorentz-Berthelot rule.[50] All interactions have been truncated to zero beyond a molecule center-based cut-off distance of

https://doi.org/10.1021/acs.jpcb.2c07572
J. Phys. Chem. B 2023, 127, 1050−1062

Table 2. Interaction Parameters of the Molecular Models Used

molecule	site	q/e	σ/Å	ε/kJ mol^{-1}
DMF	N	−0.51	3.20	0.6507
	C	0.45	3.70	0.4067
	H	0.06	2.20	0.0651
	O	−0.56	2.96	0.9134
	CH_3	0.28	3.80	0.6507
water	O	0	3.1589	0.775
	H	0.5564		
	M	−1.1128		

12 Å. The long-range part of the electrostatic interaction has been accounted for using the smooth particle mesh Ewald method,[61] while for the Lennard-Jones interaction, analytical tail correction[50] has been applied when calculating the energy and pressure.

The simulations have been performed by the GROMACS v2020 program package.[62] Equations of motion have been integrated in time steps of 2 fs. The temperature of the system has been controlled by means of a Nosé−Hoover thermostat[63,64] with a time constant of 1 ps. At the beginning of each simulation, all the molecules have been randomly placed in a rectangular basic box, the Y and Z edges of which have already been set to their final length of 50 Å, while the length of the X edge has been set to reproduce the experimental density[41] of the liquid phase. After proper energy minimization, the systems have been equilibrated for 2 ns in the (N,V,T) ensemble, followed by another 2 ns equilibration in the isothermal-isobaric (N,p,T) ensemble at 1 bar in such a way that only the X edge of the basic box has been allowed to change. Then, the interfacial systems have been created by increasing the length of the X edge to its final value of 300 Å. The interfacial systems have further been equilibrated for 10 ns in the (N,V,T) ensemble. Finally, in the production stage, two equilibrium trajectories of the lengths of 1 and 10 ns, respectively, have been generated for each system. 5000 sample configurations, separated from each other by 0.2 and 2 ps long runs, have been saved from these equilibrium trajectories for the calculation of the diffusion constant and analysis of the H-bond dynamics and for all other analyses, respectively. The surface tension values, γ, computed in the simulations are listed in Table 1.

2.2. Determination of the Intrinsic Liquid Surface. The real, capillary wave corrugated intrinsic liquid surface and the full set of molecules pertaining to it have been determined using the ITIM method.[59] In an ITIM analysis, a spherical probe is moved along test lines parallel with the macroscopic surface normal from the bulk opposite (i.e., vapor) phase toward the surface to be analyzed. Once the probe touches the first molecule pertaining to the phase of interest, the touched molecule is marked as being part of the surface layer, and the next test line is considered. The procedure results in the full list of the truly interfacial molecules (i.e., the ones that are "seen" by the probe from the opposite phase). Further, disregarding these molecules and repeating the entire procedure identifies the molecules that form the subsequent subsurface layer.[59]

The ITIM analysis has been performed using the freely available[65] Pytim software package.[66] In accordance with the findings of earlier analyses,[59,60] the radius of the spherical probe has been set to 2 Å,[59] and a 125 × 125 × 125 grid of test lines has been used; thus, the grid space between two neighboring lines has been 0.4 Å.[60] A molecule has been considered as part of the surface layer if any of its atoms has been touched by the probe sphere. In the analysis, the molecules forming the first four separate molecular layers at the liquid surface have been identified. An equilibrium snapshot of the surface portion of the equimolar system, indicating the molecules forming the first four layers beneath the liquid surface, is shown in Figure 1.

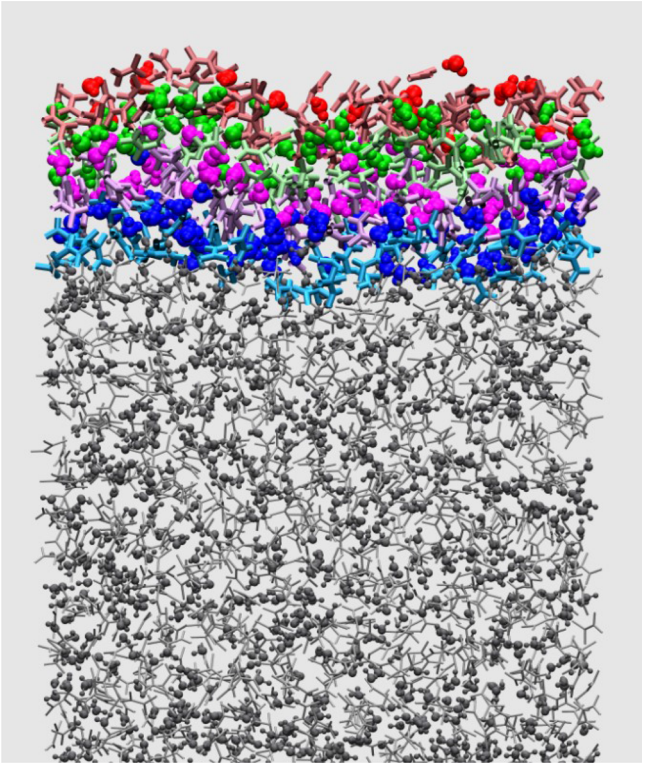

Figure 1. Equilibrium snapshot of the surface portion of the equimolar system. Red, green, magenta, and blue colors mark the molecules pertaining to the first, second, third, and fourth molecular layer beneath the liquid−vapor interface, respectively, while the molecules located beyond the fourth layer, considered here as part of the bulk liquid phase, are shown by gray color. Darker shades and balls represent water, while lighter shades and sticks represent DMF molecules.

3. RESULTS AND DISCUSSION

3.1. Relative Arrangement of the Molecules. *3.1.1. Density Profiles and Surface Adsorption.* The number density profile of the water and DMF molecules (ρ_{wat} and ρ_{DMF}, respectively) as well as the mass density profile of the entire system, ρ_{mass}, and that of the first molecular layer at the liquid surface, ρ^1_{mass}, along the surface normal axis, X, are shown in Figure 2 as obtained in systems of selected compositions. As is seen, while the water density is more or less constant up to the interfacial region, the DMF density exhibits a clear peak at the vicinity of the interface, at least in systems of small DMF concentrations. This finding suggests that DMF molecules are enriched at the vicinity of the liquid surface. To further address this point, the mole fraction of the DMF molecules in the first four individual molecular layers at the liquid surface, x^i_{DMF} (where i refers to the given layer), is plotted against the bulk liquid phase DMF mole fraction, x^b_{DMF} (as determined in the 30 Å wide slab in the middle of the liquid phase) in Figure 3.

https://doi.org/10.1021/acs.jpcb.2c07572
J. Phys. Chem. B 2023, 127, 1050−1062

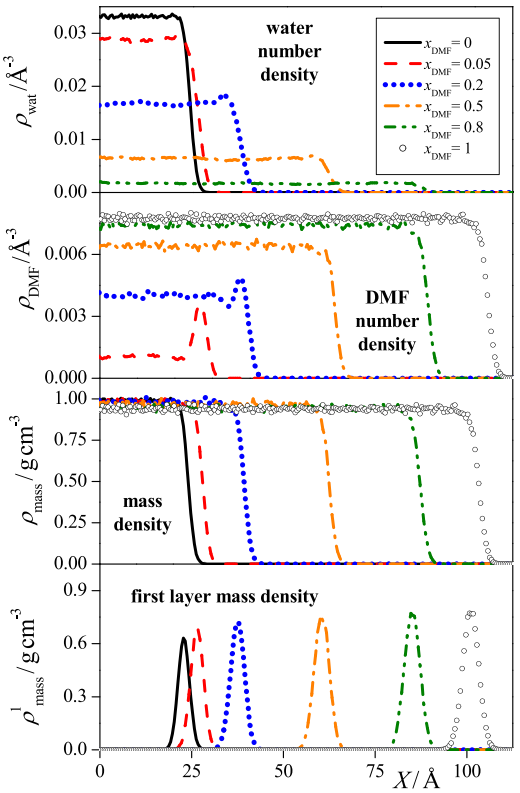

Figure 2. Number density profiles of the water (top panel) and DMF (second panel) molecules as well as mass density profiles of the entire system (third panel) and the surface molecular layer (bottom panel) along the macroscopic surface normal axis, X, as obtained in the x_{DMF} = 0 (solid black lines), x_{DMF} = 0.05 (dashed red lines), x_{DMF} = 0.2 (dotted blue lines), x_{DMF} = 0.5 (dashed−dotted orange lines), x_{DMF} = 0.8 (dashed−dotted−dotted green lines), and x_{DMF} = 1 (open circles) systems.

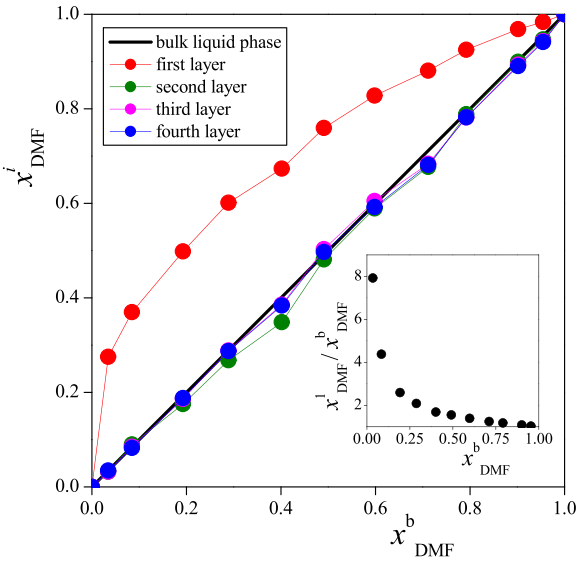

Figure 3. DMF mole fraction in the first (red), second (green), third (magenta), and fourth (blue) molecular layer beneath the liquid surface, as a function of the DMF mole fraction in the bulk liquid phase. The lines connecting the symbols are just guides to the eye. The straight black line shows the bulk liquid phase mole fraction itself for reference. The inset shows the ratio of the surface and bulk DMF mole fractions as a function of the bulk liquid phase DMF mole fraction.

The values of x^1_{DMF} and x^b_{DMF} are also collected in Table 1. As is evident, DMF is clearly enriched in the first layer, and this adsorption is progressively stronger with decreasing x^b_{DMF}. To emphasize this, we have plotted the surface enrichment (i.e., ratio of the DMF mole fractions in the surface layer and in the bulk liquid phase) as a function of the bulk DMF mole fraction in the inset of Figure 3. Contrary to the first layer, the compositions of the subsequent molecular layers agree very well with that of the bulk liquid phase. In other words, the surface adsorption of DMF involves only one molecular layer. This single layer adsorption is partly governed by the fact that exposing the apolar CH_3 groups of the DMF molecule to the vapor phase corresponds to considerably smaller free energy cost than exposing a water molecule, which loses at least one hydrogen bond at a flat surface,[59,67,68] but there is no such difference between the two molecules from the second layer on. Further, since DMF molecules can substitute water molecules in their hydrogen bonds,[3] the two molecules can mix with each other from the second layer on as much as in the bulk liquid phase. In this respect, aqueous mixtures of DMF behave similarly to those of methanol,[69] dimethylsulfoxide (DMSO),[70] acetone,[71] and methylamine,[72] i.e., molecules that also contain apolar CH_3 groups but can form H-bonds with water. On the other hand, a different behavior was observed both in the aqueous mixtures of formamide, a molecule that does not have apolar groups and hence does not adsorb at the liquid surface at all,[73] and also in those of acetonitrile[74] and HCN,[75] in which the surface structure is governed by the large dipole moment of the C≡N group, resulting in multilayer adsorption.

It is also seen from Figure 2 that the density profile of the first layer extends well into the X range of constant bulk liquid density in every system (see the two lowest panels of Figure 2). Conversely, the second and, to a small extent, even the third layer extends to the X range of intermediate densities between the liquid and vapor phases, as demonstrated in Figure 4 for systems of three different compositions. This finding stresses the importance of determining the real, capillary wave corrugated, intrinsic liquid surface when studying the surface properties of these systems, as defining the interfacial layer through the density profile as a slab of intermediate densities leads to the misidentification of a surprisingly large number of molecules as ones that are either pertaining or not pertaining to the liquid surface.

3.1.2. Relative Arrangement within the Surface. Besides analyzing the relative arrangement of the water and DMF molecules along the interface normal axis, X, we also analyze that, for the surface layer molecules, within the macroscopic plane of the surface, YZ. For this purpose, we have projected the center of the molecules belonging to the surface layer onto the YZ plane and performed Voronoi analysis[76−78] on these projections. Clearly, for a two-dimensional set of seeds, the Voronoi polygon (VP) of a seed is the locus of points in the plane that are closer to this seed than to any other one.[76−78] In our case, the seeds are the projections of the surface molecules, and hence, the area, A, of a given VP represents the surface portion that belongs to this molecule. It was shown that if the seeds are evenly distributed, the distribution of the VP area, $P(A)$, follows a gamma distribution:[79−81]

$$P(A) = aA^{\nu-1}\exp(-\nu\rho A) \quad (1)$$

https://doi.org/10.1021/acs.jpcb.2c07572
J. Phys. Chem. B 2023, 127, 1050−1062

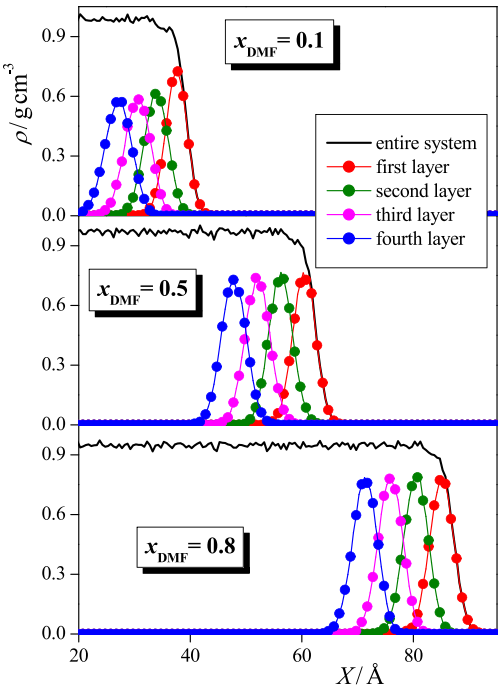

Figure 4. Mass density profile of the entire system (black) as well as of the first (red), second (green), third (magenta), and fourth (blue) molecular layers beneath the liquid surface, as obtained in the x_{DMF} = 0.1 (top panel), x_{DMF} = 0.5 (middle panel), and x_{DMF} = 0.8 (bottom panel) systems.

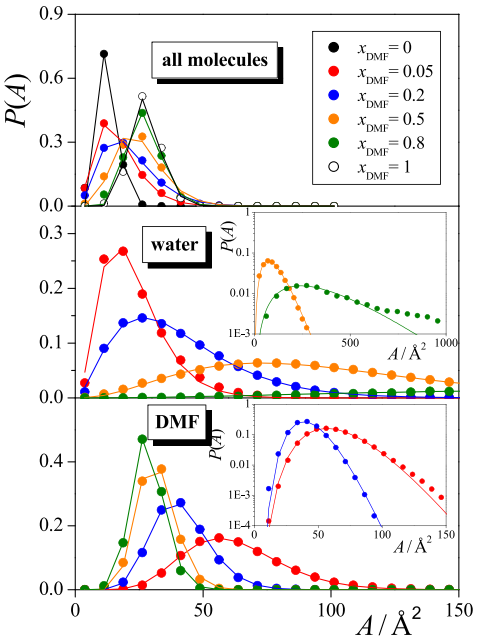

Figure 5. Area distribution of the Voronoi polygons of the surface molecules, projected to the macroscopic plane of the liquid surface, *YZ*, as obtained in the x_{DMF} = 0 (black symbols), x_{DMF} = 0.05 (red symbols), x_{DMF} = 0.2 (blue symbols), x_{DMF} = 0.5 (orange symbols), x_{DMF} = 0.8 (green symbols), and x_{DMF} = 1 (open symbols) systems when considering all molecules (top panel), only the water molecules (middle panel), and only the DMF molecules (bottom panel) of the surface layer. The lines connecting the points are just guides to the eye. The insets show the same data on a logarithmic scale.

(ν and ρ are the shape and rate parameters of the distribution, respectively, while a is a normalization constant), while in the presence of considerable density fluctuations, i.e., association between the seeds, the distribution exhibits a long tail of exponential decay at the large A side of its peak.[82] (It should be noted that, in his pioneering paper, Zaninetti suggested a Gaussian distribution in the case of evenly distributed seeds;[82] the gamma shape of the distribution is a consequence of taking into account also the requirement of $A > 0$.) Previously, we showed that even self-association of like particles in binary mixtures can be detected this way.[83] Thus, when particles of one type are disregarded and the Voronoi analysis is performed only on the particles of the other type, self-associates of the disregarded particles transform to large voids, and hence, the resulting VP area distribution exhibits the exponentially decaying tail.[83]

To investigate the possible self-association of the like molecules at the liquid surface, we have calculated the VP area distributions in the different systems simulated considering only the water, and only the DMF molecules in the different systems simulated. For reference, the $P(A)$ distribution has also been calculated taking both species into account. The resulting distributions together with their best fits by eq 1 are shown in Figure 5. The obtained distributions exhibit rather similar behavior to what has previously been seen in the bulk liquid phase of these systems.[3] Thus, the peak of the $P(A)$ distribution shifts smoothly from the position characteristic to neat water to that of neat DMF with increasing x_{DMF}, indicating that the two molecules mix with each other on the molecular scale even at the liquid surface. More importantly, the distributions obtained by disregarding one of the components follow very well the gamma distribution in almost every case. The only exception in this respect is the $P(A)$ distribution of the water molecules at the DMF-rich end of the composition range (see the upper inset of Figure 5), where the surface layer contains only very few (i.e., 5−10) water molecules in the basic box. In the presence of such a small number of water molecules, even the presence of one or two H-bonded pairs can result in a non-negligible density fluctuation and hence in a noticeable deviation from the gamma distribution, as seen also here. Our results are thus fully in accordance with what was previously seen in the bulk liquid phase:[3] the two species mix with each other on the molecular scale, forming no microheterogeneities even at the liquid surface; however, water molecules can H-bond to each other also at the surface of DMF-rich systems, even at very small surface water mole fractions.

3.2. Surface Orientation. The orientation of a surface molecule relative to the macroscopic plane of the liquid surface (or to its normal) can be unambiguously described by two independent orientational variables, and hence, a full description of their orientational statistics can be given by the joint bivariate distribution of these variables.[84,85] As it was demonstrated, the angular polar coordinates, ϑ and ϕ, of the surface normal vector in a local Cartesian frame fixed to the individual molecules represent a sufficient choice of such an independent orientational variable pair.[84,85] Here, we define the local Cartesian frames in the following way. For water, the origin of the frame coincides with the O atom, axis x is the molecular normal, axis y is parallel with the line joining the two H atoms, while axis z points along the main symmetry axis of the molecule from the O atom toward the hydrogens. Due to the C_{2v} symmetry of the water molecule, this frame is always chosen such that the inequality $\phi \leq 90°$ is satisfied. In the case

https://doi.org/10.1021/acs.jpcb.2c07572
J. Phys. Chem. B 2023, 127, 1050−1062

of DMF, the origin of the frame is the N atom, axis x points along the N−C bond from the N to the C atom, axis z is the molecular normal, while axis y is perpendicular to the other two axes, and it is oriented such that the y coordinate of the O atom is positive. Due to the planar symmetry of the DMF molecule, this frame is chosen in such a way that the relation $\vartheta \leq 90°$ (and hence $\cos\vartheta \geq 0$) holds. The definition of these local frames and those of the polar angles ϑ and ϕ of the surface normal vector, **X** (pointing, by our convention, from the liquid to the vapor phase) in these frames are illustrated in Figure 6. It should finally be emphasized that ϑ is the angle between two general spatial vectors, while ϕ is restricted to be in a pre-defined plane (i.e., the xy plane of the local frame) by definition. Therefore, domains of equal size of the variable space correspond to equal probability densities (and hence, e.g., random orientation results in uniform distribution) only if $\cos\vartheta$ and ϕ are chosen to be our variables.[84,85]

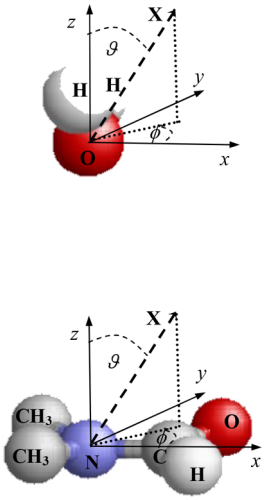

Figure 6. Definition of the local Cartesian frames fixed to the individual water (top) and DMF (bottom) molecules, as well as that of the polar angles ϑ and ϕ of the macroscopic surface normal vector, **X** (pointing, by our convention, from the liquid to the vapor phase), in these frames. O, H, C, and N atoms are shown using red, white, gray, and blue balls, respectively.

The obtained $P(\cos\vartheta,\phi)$ orientational maps of the surface layer water and DMF molecules are shown in Figure 7 (top and bottom row, respectively), as obtained in systems of selected compositions. In the two neat systems, the molecules prefer alignments in which their dipole vector lays parallel with the macroscopic plane of the liquid surface, YZ. Thus, water molecules prefer to lay parallel with the surface, as reflected in the peak of the $P(\cos\vartheta,\phi)$ orientational map at $\{\cos\vartheta = 0; \phi = 0°\}$. (It should be noted that, as it was demonstrated several times, in order to maximize their H-bonds, water molecules located at the crests and troughs of the molecularly wavy surface flip from this preferred orientation by pointing their H atoms flatly toward and away from the liquid phase, respectively.[59,68−74]) On the other hand, DMF molecules prefer to stay perpendicular to the YZ plane at the surface of their neat liquid in such a way that the CH_3 group being in the *cis* position relative to the O atom points straight to the vapor phase. In this orientation, corresponding to the $\{\cos\vartheta = 0; \phi = 120°\}$ point of the orientational map, the dipole vector of the DMF molecule, pointing roughly along the line joining the O and N atoms, stays parallel with the liquid surface. It should be noted that the peak is much sharper along the ϕ than the $\cos\vartheta$ axis of the orientational map, indicating that the main orientational preference is the parallel alignment of the molecular dipole vector with the surface plane, while the molecular plane can tip out relatively easily from the preferred perpendicular orientation. These preferred orientations, denoted here by I_w and I_{DMF}, respectively, are illustrated in Figure 8.

It is rather interesting to see that upon diluting both liquids with the other component, the orientational preferences of

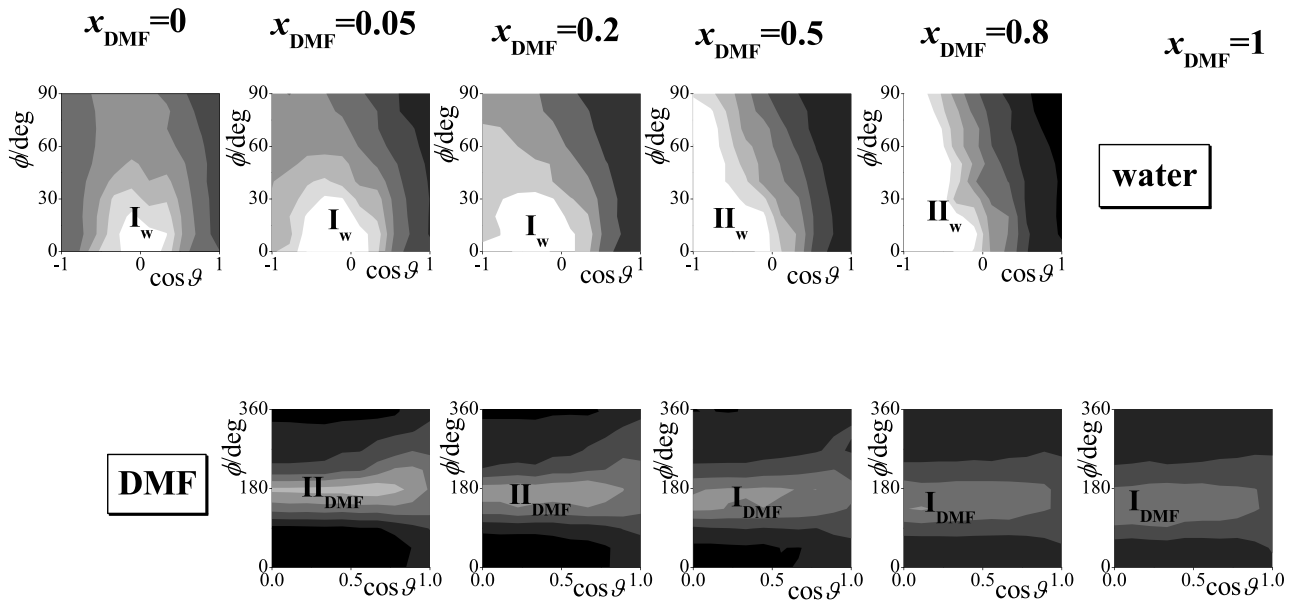

Figure 7. Orientational maps of the surface water (top row) and DMF (bottom row) molecules, as obtained in the $x_{DMF} = 0$ (first column), $x_{DMF} = 0.05$ (second column), $x_{DMF} = 0.2$ (third column), $x_{DMF} = 0.5$ (fourth column), $x_{DMF} = 0.8$ (fifth column), and $x_{DMF} = 1$ (sixth column) systems. Lighter colors correspond to higher probabilities.

https://doi.org/10.1021/acs.jpcb.2c07572
J. Phys. Chem. B 2023, 127, 1050−1062

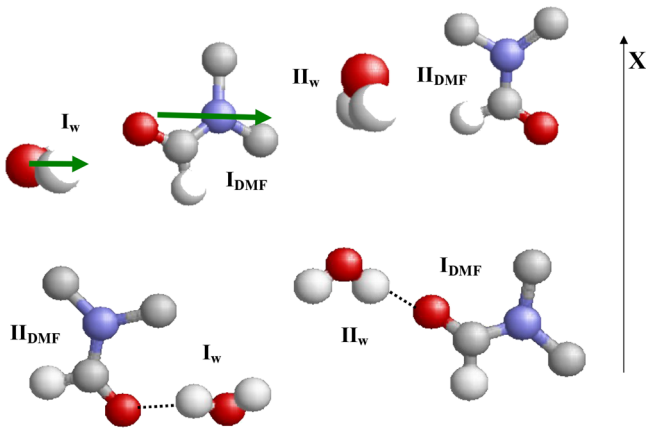

Figure 8. Top: illustration of the orientations preferred by the water and DMF molecules in the surface layer. Bottom: H-bonding pairs of surface water and DMF molecules, both of which are aligned in one of their preferred orientations, as taken out from equilibrium configurations. Color-coding of the atoms is the same as in Figure 6; the green arrows indicate the direction of the molecular dipole vectors. **X** is the surface normal vector pointing from the liquid to the vapor phase.

their molecules undergo certain changes. Thus, upon adding DMF to water, the peak of the $P(\cos\vartheta,\phi)$ map of the water molecules gradually shifts to $\cos\vartheta = -1$. (In the case of $\cos\vartheta = -1$, the projection of **X** onto the xy pane of the local frame becomes a point, and hence, angle ϕ loses its meaning, see Figure 6). In this orientation, marked here by II_w, the water molecule stays perpendicular to the liquid surface, pointing both its H atoms symmetrically to the liquid phase (see Figure 8). This orientational preference is triggered by the preferred I_{DMF} alignment of the DMF molecules in systems where DMF is the major component of the surface layer because a water molecule of alignment II_w can form a H-bond with a DMF molecule of alignment I_{DMF}, as also shown in Figure 8. On the other hand, in systems where the major surface component is water, the peak of the DMF $P(\cos\vartheta,\phi)$ map shifts to $\{\cos\vartheta = 0; \phi = 180°\}$. In the corresponding alignment, denoted here as II_{DMF}, the DMF molecule still stays perpendicular to the surface, but now the two CH_3 groups point symmetrically away from the liquid phase, as illustrated in Figure 8. It should again be noted that, similarly to I_{DMF}, the peak of this preferred alignment is also noticeably sharper along the ϕ than the $\cos\vartheta$ axis. This orientational preference can be rationalized by considering that, in order to minimize the surface tension of the system, as many CH_3 groups should be exposed to the vapor phase as possible. Further, in this alignment, the DMF molecule can accept a H-bond from a water molecule of alignment I_w. This H-bonding pattern is also illustrated in Figure 8.

3.3. Hydrogen Bonding at the Liquid Surface. As our results have revealed that the surface orientation of both molecules is governed, at least partly, by the requirement of forming as many H-bonds with each other as possible, here we analyze the properties, namely, the connectivity and lifetime of the H-bonds at the liquid surface. In the following analyses, a molecule pair is regarded to form a H-bond if the distance of the donor and acceptor O atoms is less than 3.5 Å, and the distance of the bonding H atom from the acceptor O atom is less than 2.45 Å.[3] Since these cut-off distances are the first minimum positions of the respective radial distribution functions (see Figures 1−3 of ref 3.), this definition is free from any arbitrarily chosen parameter.

3.3.1. Connectivity of the Hydrogen Bonds. Similarly to bulk water,[86,87] H-bonds form an infinite, percolating network also at the surface of liquid water under ambient conditions.[88−90] The breaking down of this percolating network at high temperatures was recently found to be the physical reason behind the surface tension anomaly of water.[89,90] However, due to the lack of donable H atoms of the DMF molecule, the addition of DMF to water also leads to the breakdown of this percolating surface network of the H-bonds. To investigate the occurrence of this breakdown, we have calculated the distribution of the size, n, of the H-bonding clusters of the surface molecules in the different systems simulated (where the "size" of a cluster simply means the number of molecules belonging to it).

At the percolation threshold, the cluster size distribution follows a power law:

$$P(n) \sim n^{-\alpha} \tag{2}$$

with the universal exponent $\alpha = 2.05$ in two-dimensional systems.[91] In non-percolating systems, $P(n)$ quickly drops below this critical line and remains there in the entire n range, while in the case of a percolating system, $P(n)$ exceeds the critical line at large n values.

The $P(n)$ distributions obtained at the surface of neat water as well as of the $x_{DMF} = 0.05$ system are shown, together with the critical line of eq 2, in Figure 9. As is seen, while the H-bond network of the surface molecules clearly percolates in neat water, at the surface of the $x_{DMF} = 0.05$ system, this network is already broken. This finding is understandable considering that while the bulk liquid phase DMF mole percentage of this system is only 3.2%, in the surface layer this value is already as large as 27.5% (see Table 1). In other words, due to the rather strong surface adsorption of the DMF molecules, the infinite, percolating H-bond network of the surface molecules breaks down already at very low bulk phase DMF mole fractions. It should also be emphasized that, in this respect, DMF behaves in a completely different way from its double demethylated analogue, i.e., formamide, which can also donate bonding H atoms, and therefore, the H-bond network

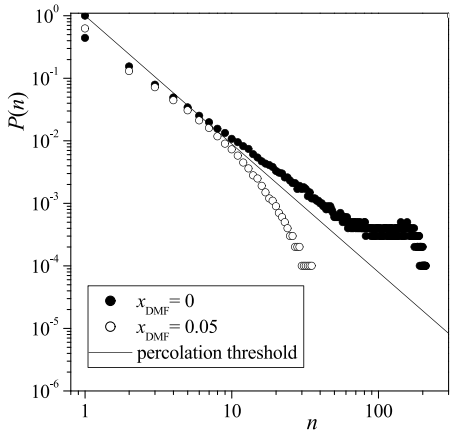

Figure 9. Size distribution of the H-bonded clusters in the surface layer of neat water (full symbols) and of the $x_{DMF} = 0.05$ system (open symbols). The critical line of eq 2 marking the percolation threshold is also shown (solid line).

https://doi.org/10.1021/acs.jpcb.2c07572
J. Phys. Chem. B 2023, 127, 1050−1062

of the surface molecules remains percolating in the entire composition range of water−formamide mixtures.[73]

3.3.2. Lifetime of the Surface Hydrogen Bonds. The lifetime of H-bonds can be fully characterized by their survival probability, $L_{HB}(t)$; i.e., the probability that a H-bond that exists at t_0 remains uninterruptedly intact until $t + t_0$. Since the breaking of a H-bond, like any decomposition reaction, follows first-order kinetics, the $L_{HB}(t)$ distribution is of exponential decay. Further, since H-bonds can, in general, break by two different mechanisms, i.e., either temporarily due to the vibrational (H-bond stretching) or permanently due to the translational/rotational motion of the participating molecules, the $L_{HB}(t)$ function is expected to have the bi-exponential form:

$$L_{HB}(t) = A_1\exp(-t/\tau_{HB}^{vib}) + A_2\exp(-t/\tau_{HB}) \quad (3)$$

where τ_{HB}^{vib} and τ_{HB} are the characteristic times of the processes corresponding to the temporary (vibrational) and permanent breaking of the H-bonds, respectively. Further, since $\tau_{HB}^{vib} \ll \tau_{HB}$, the value of τ_{HB} can be regarded as a good approximation of the mean lifetime of the H-bonds. The values of τ_{HB} have been determined by fitting eq 3 to the obtained $L_{HB}(t)$ data. To increase the accuracy of their determination, the data corresponding to the first 1 ps have been omitted from the fitting procedure.

The $L_{HB}(t)$ data together with their bi-exponential fits are shown in Figure 10, as obtained for the surface water−water and water−DMF H-bonds in selected systems. Further, the mean lifetimes of the water−water and water−DMF H-bonds in the surface layer of the systems simulated, τ_{HB}, are collected in Table 1. For reference, the mean bulk lifetime of these H-bonds, calculated beyond the fourth subsurface layer, is also given. It should be noted that, at the DMF-rich end of the composition range, the $L_{HB}(t)$ curves of the water−water H-bonds become increasingly noisy, and hence, the corresponding τ_{HB} values become increasingly inaccurate due to the fact that very few water molecules are present in these systems. The composition dependence of the H-bond mean lifetimes does not show a clear trend; nevertheless, our data suggest that they go through a maximum in the surface DMF mole fraction range of 0.6−0.9. More importantly, it is seen that water−DMF H-bonds live, on average, 25−60% longer than water−water H-bonds at the liquid surface. As it was shown several times, the mean lifetime of a H-bond is not related to its strength.[92−94] Instead, this difference is likely related to the somewhat smaller mobility and considerably longer surface residence time of the DMF molecules than those of waters (see the next subsection). A similar but smaller (i.e., only about 10−20%) difference is seen between the mean lifetime of these two types of H-bonds in the bulk liquid phase. Further, it is also clear that both types of H-bonds live considerably, i.e., 2−5 times longer in the bulk liquid phase than at the liquid surface. This difference was shown to be caused by the enhanced mobility of the molecules at the liquid surface.[94]

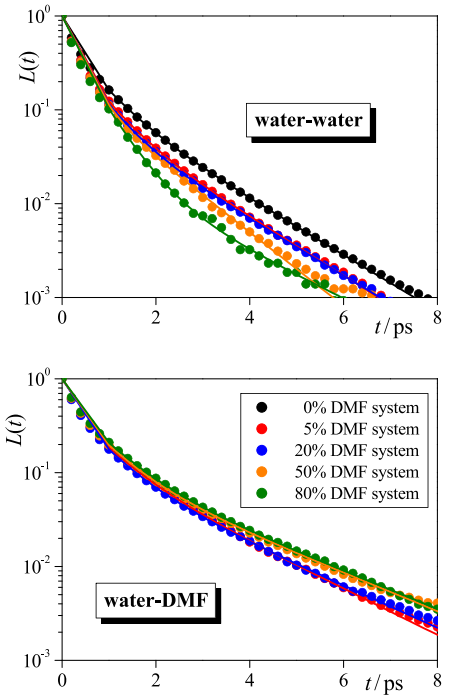

Figure 10. Survival probability of the water−water (top panel) and water−DMF (bottom panel) H-bonds in the surface layer of the x_{DMF} = 0 (black symbols), x_{DMF} = 0.05 (red symbols), x_{DMF} = 0.2 (blue symbols), x_{DMF} = 0.5 (orange symbols), and x_{DMF} = 0.8 (green symbols) systems. Solid lines show the bi-exponential fit (eq 3) to the data points. To emphasize the exponential decay of the data and the quality of the fits, the results are shown on a logarithmic scale.

3.4. Surface Dynamics. *3.4.1. Residence Time of the Molecules at the Liquid Surface.* The survival probability, $L(t)$, and mean residence time, τ_{surf}, of the molecules in the surface layer can be defined in an analogous way to the survival probability and mean lifetime of the H-bonds. Thus, $L(t)$ is the probability that a molecule belonging to the surface layer at t_0 remains uninterruptedly there up to $t + t_0$. Since the departure from the liquid surface is also a process of first-order kinetics, and it can, again, happen by two different mechanisms (i.e., temporarily due to the oscillatory and permanently due to the diffusive motion of the given molecule), $L(t)$ is also expected to follow bi-exponential decay:

$$L(t) = A_1\exp(-t/\tau_{osc}) + A_2\exp(-t/\tau_{surf}) \quad (4)$$

where τ_{osc} and τ_{surf}, respectively, are the time scales of these processes. Further, since $\tau_{osc} \ll \tau_{surf}$, the value of τ_{surf} can be used as a good estimate of the mean residence time of the molecules in the surface layer. The importance of determining τ_{surf} stems from the fact that its value sets the time scale on which surface processes can be meaningfully discussed. Namely, for processes occurring on time scales shorter than τ_{surf}, surface and non-surface molecules can be distinguished from each other, and hence, the given process can be meaningfully discussed considering specifically the surface particles. On the other hand, in processes occurring on time scales longer than τ_{surf}, the molecules can leave the surface layer and re-enter to it several times during this process, and hence, from the point of view of this process, distinguishing between surface and non-surface particles is meaningless.

The $L(t)$ survival probabilities of the water and DMF molecules are shown, together with their bi-exponential fits, in Figure 11 as obtained in selected systems. Further, the mean surface residence time values of both the water and DMF molecules are collected in Table 1. As is seen, DMF molecules stay at least an order of magnitude longer at the liquid surface than water molecules, and this difference is larger in systems of smaller DMF mole fractions. This finding is emphasized in the inset of Figure 11, showing the ratio of the τ_{surf} values corresponding to the DMF and water molecules (τ_{surf}^{DMF} and

https://doi.org/10.1021/acs.jpcb.2c07572
J. Phys. Chem. B 2023, 127, 1050−1062

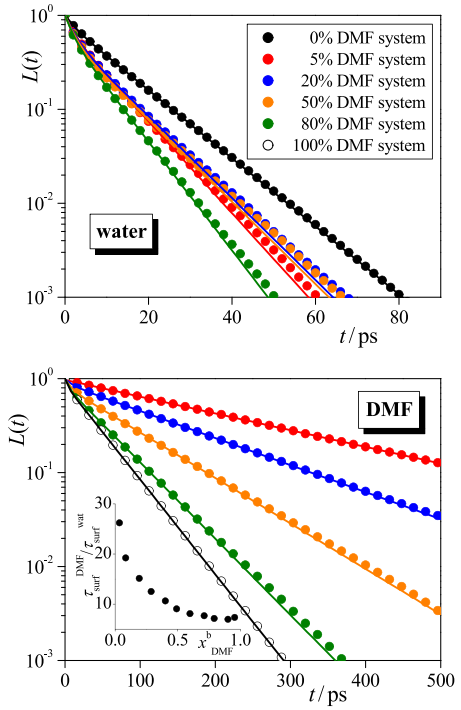

Figure 11. Survival probability of the water (top panel) and DMF (bottom panel) molecules in the surface layer of the $x_{DMF} = 0$ (black symbols), $x_{DMF} = 0.05$ (red symbols), $x_{DMF} = 0.2$ (blue symbols), $x_{DMF} = 0.5$ (orange symbols), $x_{DMF} = 0.8$ (green symbols), and $x_{DMF} = 1.0$ (open symbols) systems. Solid lines show the bi-exponential fit (eq 4) to the data points. To emphasize the exponential decay of the data and the quality of the fits, the results are shown on a logarithmic scale. The inset shows the ratio of the mean surface residence times of the DMF and water molecules as a function of the bulk liquid phase DMF mole fraction.

τ^{wat}_{surf}, respectively) as a function of x^b_{DMF}. This finding can largely be attributed to the behavior of the DMF molecules, as their mean surface residence time clearly and markedly increases with their decreasing mole fraction. The physical reason behind this behavior is that, with the decreasing DMF mole fraction, the H-bonded clusters at the liquid surface become larger, and larger fractions of the surface DMF molecules participate in such clusters. Thus, with their decreasing mole fraction, DMF molecules become increasingly tethered by their H-bonds, formed with water molecules, to the liquid surface, hindering thus their departure from the surface layer.

On the other hand, the mean surface residence time of the surface water molecules does not exhibit a clear trend up to $x^b_{DMF} = 0.4$ (i.e., $x^1_{DMF} \approx 0.7$), while above this value it decreases with the increasing DMF mole fraction. This behavior can also be explained by the gradual breakdown of the H-bonding clusters: while H-bonded water clusters built up by more than three molecules persist up to a DMF mole fraction of about 0.7,[3] a further increase of the DMF mole fraction in the surface layer leads to the appearance of an increasing fraction of isolated (i.e., forming no H-bonds) water molecules and thus to the enhancement of the exchange of water between the surface layer and bulk liquid phase. It should be noted that very similar behavior was observed earlier at the surface of water−methylamine mixtures.[72]

3.4.2. Surface Diffusion. In homogeneous, isotropic systems, the diffusion coefficient of the molecules can be calculated through the Einstein relation:[50,81]

$$D = \frac{\langle (\mathbf{r}_i(t_0 + t) - \mathbf{r}_i(t_0))^2 \rangle}{2dt} \quad (5)$$

where $\mathbf{r}_i(t_0 + t)$ and $\mathbf{r}_i(t_0)$ denote the position vectors of particle i at the times $t_0 + t$ and t_0, respectively, the parameter d is simply the dimensionality of the diffusive motion, and the angled brackets <···> denote ensemble averaging. It should be noted that the numerator in eq 5 is often referred to as the mean square displacement of the particles and denoted by MSD.

The mobility of the molecules within the surface layer of the systems simulated is characterized here by their lateral diffusion coefficient, $D_{||}$, calculated by defining MSD within the macroscopic plane of the liquid surface, YZ, using $d = 2$ in eq 5, and fitting a straight line to the MSD vs t data obtained from the simulations (the steepness of which being $2dD_{||}$, see eq 5). No Yeh-Hummer correction[95] has been applied in the calculation. In order to ensure that the molecules have already left the ballistic regime and indeed perform diffusive motion, the first 3 ps of the MSD(t) data have been left out from the fitting procedure. It should be noted that molecular trajectories have only been considered in the calculation of the MSD(t) data as long as the corresponding molecule has remained within the surface layer.

The time scale of this lateral diffusion, τ_D, is defined as the time during which surface molecules explore an area within the YZ plane that is equal to the average surface area per molecule, A_m, i.e.,[81,96]

$$\tau_D = \frac{A_m}{4D_{||}} \quad (6)$$

where

$$A_m = \frac{2L_Y L_Z}{<N_{surf}>} \quad (7)$$

L_Y and L_Z being the lengths of the Y and Z edges of the basic box, respectively, $<N_{surf}>$ is the mean number of the surface molecules, and the factor 2 in the numerator of eq 7 stands for the two liquid−vapor interfaces present in the basic box. Due to the large difference in their size, water and DMF molecules occupy markedly different portions of the liquid surface. Therefore, we have estimated the value of A_m for the water and DMF molecules by those obtained in the respective neat systems, i.e., 12.1 Å^2 and 27.5 Å^2, respectively.

The MSD vs t data of the two molecules are shown, along with their linear fits, in Figure 12 as obtained in selected systems. Further, the $D_{||}$ and τ_D values of the water and DMF molecules are collected in Table 1. For reference, the three-dimensional bulk liquid phase diffusion coefficients, calculated beyond the fourth subsurface layer, are also given. As is seen, the characteristic time of the surface diffusion of the DMF molecules, τ_D, is considerably (i.e., 3−8 times) smaller than their mean surface residence time in the entire composition range, indicating that DMF molecules indeed perform considerable lateral diffusion during their stay at the liquid surface. However, for the water molecules, the values of τ_D and τ_{surf} are comparable with each other in the surface DMF mole fraction range of about 0.25−0.75. In other words, the diffusive motion of the water molecules at the surface of these systems is

https://doi.org/10.1021/acs.jpcb.2c07572
J. Phys. Chem. B 2023, 127, 1050−1062

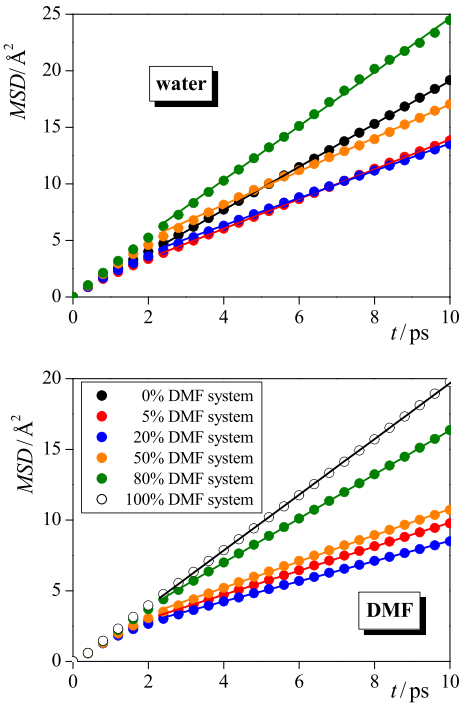

Figure 12. Lateral mean square displacement of the water (top panel) and DMF (bottom panel) molecules in the surface layer of the x_{DMF} = 0 (black symbols), x_{DMF} = 0.05 (red symbols), x_{DMF} = 0.2 (blue symbols), x_{DMF} = 0.5 (orange symbols), x_{DMF} = 0.8 (green symbols), and x_{DMF} = 1 (open symbols) systems. Solid lines show the linear fits to the data points.

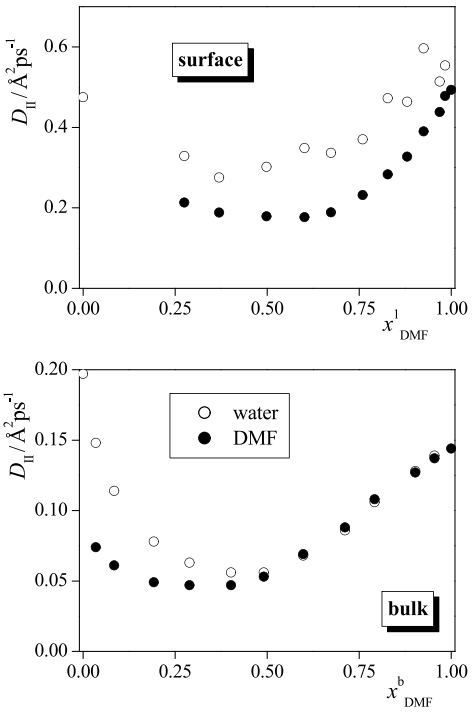

Figure 13. Dependence of the lateral diffusion coefficient of the surface molecules within the macroscopic plane of the interface, *YZ*, on the surface composition (top), and that of the three-dimensional bulk phase diffusion coefficient on the bulk composition (bottom), as obtained for the water (open symbols) and DMF (filled symbols) molecules.

limited to an area roughly equal to the average surface area they occupy, A_m.

The comparison of the surface and bulk diffusion coefficient values clearly reveals that both species exhibit enhanced surface mobility, as the surface diffusion coefficient of both molecules is about 2−6 times larger than their three-dimensional bulk diffusion coefficient in every case. This enhanced surface mobility, being in a clear accordance with the observed shorter lifetime of the H-bonds at the surface than in the bulk (see Subsection 3.3.2), is due to the lack of steric constraints on the surface molecules from the vapor phase.[81,94] It is also seen that, in spite of the fact that the $D_{||}$ value of the DMF molecules at the surface of their neat system is similar to that of water (i.e., 0.49 vs 0.48 Å^2/ps, see Table 1), the lateral diffusion coefficient of the water molecules is noticeably larger, possibly due to their smaller size and hence larger mobility, than those of the DMF molecules at the surface of every mixed system.

Finally, it is interesting to note that the lateral diffusion coefficient of both molecules goes through a minimum around the surface DMF mole fraction value of 0.6, as illustrated in Figure 13. Similar behavior is seen in the bulk liquid phase, where the minimum occurs at somewhat smaller DMF mole fraction values (see Figure 13). In other words, both components slow down the diffusion of the other one. In the case of DMF, this water-induced slowing down can be explained by the H-bond formation between the DMF and water molecules, while the slowing down of water in the presence of DMF is likely caused by steric hindrances imposed by the neighboring bulky DMF molecules.

4. CONCLUSIONS

In this paper, we have investigated the molecular level structure and dynamics of the liquid−vapor interface of DMF−water mixtures, spanning the entire composition range, in detail. The interfacial properties are found to be determined by (i) the fact that the aprotic dipolar DMF molecule bears also apolar (i.e., CH_3) groups and (ii) the ability of the aprotic DMF molecules of accepting H-bonds from water. Thus, DMF is found to be strongly adsorbed at the surface of its aqueous mixtures, but this adsorption is strictly monomolecular. The driving force of this adsorption is to expose as many CH_3 groups instead of water molecules to the vapor phase as possible. Such a driving force can, however, only act in the first molecular layer at the liquid surface. Not surprisingly, similar monolayer adsorption was found earlier in the aqueous solutions of other solutes of H-bonding ability that contain also at least one CH_3 group, such as methanol,[69] DMSO,[70] acetone,[71] and methylamine.[72] Apart from this enrichment of DMF in the surface layer, the two molecules are found, similarly to the bulk liquid phase,[3] to mix with each other even on the molecular scale. Thus, no marked self-association of the like molecules is observed even at the liquid surface.

Although DMF molecules can replace water molecules in their H-bonds, the lack of H-donating ability of DMF leads to the rapid disruption of the percolating H-bond network at the liquid surface with the increasing DMF concentration. Due to the aforementioned strong adsorption of DMF, this breaking up of the surface H-bond network occurs below a bulk phase DMF mole fraction of 0.03. This disruption of the surface H-bond network also affects the mean surface residence time of both types of molecules. Thus, with the increasing DMF mole

https://doi.org/10.1021/acs.jpcb.2c07572
J. Phys. Chem. B 2023, 127, 1050−1062

fraction, the surface residence time of both species decreases (although, for water, such a decrease is only apparent above a bulk DMF mole fraction of 0.4) due to the increasing fraction of surface molecules having no H-bonded neighbors within the surface layer. Again, very similar behavior was previously seen at the surface of water−methylamine mixtures.[72]

The possibility of H-bond formation between unlike molecules influences the orientational preferences of the surface molecules, as well. Thus, the major surface component always prefers such an orientation in which the molecular dipole vector lays parallel with the macroscopic plane of the liquid surface. However, the orientational preference of the minor component is governed, at both ends of the composition range, by the possibility of forming a H-bond with a molecule of the major component at the liquid surface.

The characteristic time of the breaking and re-formation of the H-bonds at the surface is found to be considerably smaller, while that of the surface diffusion is somewhat smaller than or, at least, comparable with the mean surface lifetime of the corresponding molecules; therefore, both processes can be discussed as occurring at the liquid surface. The mean lifetime of the water−DMF H-bonds is found to be noticeably longer than those of the water−water H-bonds both at the liquid surface and in the bulk. Further, due to the enhanced mobility of the molecules at the liquid surface,[94] both types of H-bonds live 2−5 times longer in the bulk liquid phase than at the surface. Consistently, the lateral diffusion coefficient of both species at the surface is found to be 2−6 times larger than the corresponding bulk phase value. Finally, it is found that the diffusion of both molecules slows down in the presence of the other one. In the case of DMF, this effect is caused by the possibility of their H-bond formation with their water neighbors, while in the case of water, steric hindrances caused by the bulky DMF neighbors are responsible for this slowing down.

AUTHOR INFORMATION

Corresponding Author

Pál Jedlovszky − *Department of Chemistry, Eszterházy Károly University, H-3300 Eger, Hungary;* orcid.org/0000-0001-9304-435X; Email: jedlovszky.pal@uni-eszterhazy.hu

Authors

Barbara Honti − *Department of Organic Chemistry and Technology, Budapest University of Technology and Economics, Budapest 1111, Hungary*

Balázs Fábián − *Department of Theoretical Biophysics, Max Planck Institute of Biophysics, Frankfurt am Main 60438, Germany*

Abdenacer Idrissi − *University of Lille, CNRS UMR 8516 -LASIRe - Laboratoire Avancé de Spectroscopie pour les Interactions la Réactivité et l'environnement, 59000 Lille, France;* orcid.org/0000-0002-6924-6434

Complete contact information is available at: https://pubs.acs.org/10.1021/acs.jpcb.2c07572

Notes

The authors declare no competing financial interest.

ACKNOWLEDGMENTS

P.J. acknowledges financial support from the NKFIH Foundation, Hungary (project No. 134596).

REFERENCES

(1) Jorgensen, W. L.; Swenson, C. J. Optimized Intermolecular Potential Functions for Amides and Peptides. Structure and Properties of Liquid Amides. *J. Am. Chem. Soc.* **1985**, *107*, 569−578.

(2) Lei, Y.; Li, H.; Pan, H.; Han, S. Structures and Hydrogen Bonding Analysis of N,N-Dimethylformamide and N,N-Dimethylformamide−Water Mixtures by Molecular Dynamics Simulations. *J. Phys. Chem. A* **2003**, *107*, 1574−1583.

(3) Koverga, V.; Juhász, Á.; Dudariev, D.; Lebedev, M.; Idrissi, A.; Jedlovszky, P. Local Structure of DMF-Water Mixtures, as Seen from Computer Simulations and Voronoi Analysis. *J. Phys. Chem. B* **2022**, *126*, 6964−6978.

(4) Kumbharkhane, A. C.; Puranik, S. M.; Mehrotra, S. C. Dielectric Relaxation Studies of Aqueous N,N-Dimethylformamide Using a Picosecond Time Domain Technique. *J. Sol. Chem.* **1993**, *22*, 219−229.

(5) Jia, G. Z.; Huang, K. M.; Yang, X. Q.; Song, J. P.; Yang, L. J. Specific Phenomenon of Effective Permittivity for DMF-H_2O Solution. *Acta Phys.-Chim. Sin.* **2009**, *25*, 1906−1910.

(6) Honti, B.; Idrissi, A.; Jedlovszky, P. Calculation of the Free Energy of Mixing As a Tool for Assessing and Improving Potential Models. The Case of the N,N-Dimethylformamide − Water System. *J. Phys. Chem. B* **2021**, *125*, 4819−4830.

(7) Puhovski, Y. P.; Rode, B. M. Molecular Dynamics Simulations of Aqueous Formamide Solution. 2. Dynamics of Solvent Molecules. *J. Chem. Phys.* **1995**, *102*, 2920−2927.

(8) Elola, M. D.; Ladanyi, B. M. Intermolecular Polarizability Dynamics of Aqueous Formamide Liquid Mixtures Studied by Molecular Dynamics Simulations. *J. Chem. Phys.* **2007**, *126*, No. 084504.

(9) Kiss, B.; Fábián, B.; Idrissi, A.; Szőri, M.; Jedlovszky, P. Miscibility and Thermodynamics of Mixing of Different Models of Formamide and Water in Computer Simulation. *J. Phys. Chem. B* **2017**, *121*, 7147−7155.

(10) Kiss, B.; Fábián, B.; Idrissi, A.; Szőri, M.; Jedlovszky, P. Correction to "Miscibility and Thermodynamics of Mixing of Different Models of Formamide and Water in Computer Simulation". *J. Phys. Chem. B* **2017**, *121*, 9319.

(11) Lilley, T. H. Thermodynamics of Peptides and Model Systems. In *Biochemical Thermodynamics*; Jones, M. N., Ed.; Elsevier: Amsterdam, 1988.

(12) Eberhardt, E. S.; Raines, R. T. Amide-Amide and Amide-Water Hydrogen Bonds: Implications for Protein Folding and Stability. *J. Am. Chem. Soc.* **1994**, *116*, 2149−2150.

(13) Vargas, R.; Garza, J.; Dixon, D. A.; Hay, B. P. How Strong Is the Cα−H···OC Hydrogen Bond? *J. Am. Chem. Soc.* **2000**, *122*, 4750−4755.

(14) Basu, S.; Agarwal, A. K.; Jassal, M. Concept of Minimum Electrospinning Voltage in Electrospinning of Polyacrylonitrile N, N-Dimethylformamide System. *J. Appl. Polym. Sci.* **2011**, *122*, 856−866.

(15) Molnár, K.; Juriga, D.; Nagy, P. M.; Sinkó, K.; Jedlovszky-Hajdu, A.; Zrínyi, M. Electrospun Poly(Aspartic Acid) Gel Scaffolds for Artificial Extracellular Matrix. *Polym. Int.* **2014**, *63*, 1608−1615.

(16) Azahar Ali, M.; Mondal, K.; Singh, C.; Malhotra, B. D.; Sharma, A. Anti-Epidermal Growth Factor Receptor Conjugated Mesoporous Zinc Oxide Nanofibers for Breast Cancer Diagnostics. *Nanoscale* **2015**, *7*, 7234−7245.

(17) Molnár, K.; Jedlovszky-Hajdu, A.; Zrínyi, M.; Jiang, S.; Agarwal, S. Poly(amino acid)-Based Gel Fibers with pH Responsivity by Coaxial Reactive Electrospinning. *Macromol. Rapid Commun.* **2017**, *38*, No. 1700147.

(18) Barczikai, D.; Kacsari, V.; Domokos, J.; Szabó, D.; Jedlovszky-Hajdu, A. Interaction of Silver Nanoparticle and Commonly Used Anti-Inflammatory Drug Within a Poly(Amino Acid) Derivative Fibrous Mesh. *J. Mol. Liq.* **2021**, *322*, No. 114575.

(19) Farina, G.; Romanin, A.; Capobianco, G.; Torzo, F. Electrochemical Reduction Mechanism of Phtalimide and Some of Its N-Derivates in DMF. *J. Electroanal. Chem. Interfacial Electrochem.* **1971**, *33*, 31−44.

(20) Keeley, G. P.; O'Neill, A.; Holzinger, M.; Cosiner, S.; Coleman, J. N.; Duesberg, G. S. DMF-Exfoliated Graphene for Electrochemical NADH Detection. *Phys. Chem. Chem. Phys.* **2011**, *13*, 7747−7750.
(21) Pandit, S. A.; Rather, M. A.; Bhat, S. A.; Jan, R.; Rather, G. M.; Bhat, M. A. An Insight into a Fascinating DMF-Water Mixed Solvent System: Physicochemical and Electrochemical Studies. *ChemistrySelect* **2017**, *2*, 5115−5127.
(22) Rodríguez-Gattorno, G.; Santiago-Jacinto, P.; Rendon-Vázquez, L.; Németh, J.; Dékány, I.; Díaz, D. Novel Synthesis Pathway of ZnO Nanoparticles from the Spontaneous Hydrolysis of Zinc Carboxylate Salts. *J. Phys. Chem. B* **2003**, *107*, 12597−12604.
(23) Vázquez-Olmos, A.; Redón, R.; Rodríguez-Gattorno, G.; Mata-Zamora, M. E.; Morales-Leal, F.; Fernández-Osorio, A.; Saniger, J. M. One-Step Synthesis of Mn_3O_4 Nanoparticles: Structural and Magnetic Study. *J. Colloid Interface Sci.* **2005**, *291*, 175−180.
(24) Aguirre, M. E.; Rodríguez, H. B.; San Román, E.; Feldhoff, A.; Grela, M. A. Ag@ZnO Core−Shell Nanoparticles Formed by the Timely Reduction of Ag^+ Ions and Zinc Acetate Hydrolysis in N,N-Dimethylformamide: Mechanism of Growth and Photocatalytic Properties. *J. Phys. Chem. C* **2011**, *115*, 24967−24974.
(25) Meth-Cohn, O.; Stanforth, S. P. The Vilsmeier-Haack Reaction. *Compr. Org. Synthes.* **1991**, *2*, 777−794.
(26) Grosjean, N.; Descorme, C.; Besson, M. Catalytic Wet Air Oxidation of N,N-Dimethylformamide Aqueous Solutions: Deactivation of TiO2 and ZrO2-Supported Noble Metal Catalysts. *Appl. Catal. B: Environ.* **2010**, *97*, 276−283.
(27) Yang, X.; Clark, A. E. Preferential Solvation of Metastable Phases Relevant to Topological Control Within the Synthesis of Metal−Organic Frameworks. *Inorg. Chem.* **2014**, *53*, 8930−8940.
(28) Ghosh, S.; Pal, S.; Rajamanickam, S.; Shome, R.; Mohanta, P. R.; Ghosh, S. S.; Patel, B. K. Access to Multifunctional AEEgens via Ru(II)-Catalyzed Quinoxaline-Directed Oxidative Annulation. *ACS Omega* **2019**, *4*, 5565−5577.
(29) Desai, K. G.; Desai, K. R. A Facile Microwave Enhanced Synthesis of Sulfur-Containing 5-Membered Heterocycles Derived from 2-Mercaptobenzothiazole over $ZnCl_2$/DMF and Antimicrobial Activity Evaluation. *J. Sulfur Chem.* **2006**, *27*, 315−328.
(30) Caddick, S.; Fitzmaurice, R. Microwave Enhanced Synthesis. *Tetrahedron* **2009**, *65*, 3325−3355.
(31) Keglevich, G.; Grun, A.; Bálint, E. Microwave Irradiation and Phase Transfer Catalysis in C-, O- and N-Alkylation Reactions. *Curr. Org. Chem.* **2013**, *10*, 751−763.
(32) Bálint, E.; Kállai, M.; Kovács, O.; Bölcskei, H.; Keglevich, G. O-Arylation of Iodophenols with 2-Fluorobenzaldehyde under Microwave Conditions. *Lett. Drug Des. Discov.* **2014**, *11*, 114−120.
(33) Ergin, S. P. The Effect of Temperature on Association Constants and Conductivities of Ferrous Chloride and Ferric Chloride in DMF-Water Mixtures. *Eur. J.Chem.* **2012**, *3*, 399−403.
(34) Ohara, M.; Takagaki, A.; Nishimura, S.; Ebitani, K. Syntheses of 5-Hydroxymethylfurfural and Levoglucosan by Selective Dehydration of Glucose Using Solid Acid And Base Catalyst. *Appl. Catal. A Gen.* **2020**, *383*, 149−155.
(35) Bipp, H.; Kieczka, H. Formamides. In *Ullman's Encyclopedia of Industrial Chemistry*; Wiley-VCH: Weinheim, 2002.
(36) Weingärtner, H.; Holz, M.; Hertz, H. G. Some Structural Aspects in Binary Aqueous Mixtures of Simple Amides from Rotational Molecular Motions. *J. Solution Chem.* **1978**, *7*, 689−704.
(37) Cilense, M.; Benedetti, A. V.; Vollett, D. R. Thermodynamic Properties of Liquid Mixtures II. Dimethylformamide-Water. *Thermochim. Acta* **1983**, *63*, 151−156.
(38) Volpe, C. D.; Guarino, G.; Sartorio, R.; Vitagliano, V. Diffusion, Viscosity, and Refractivity Data on the System Dimethylformamide-Water at 20 and 40 °C. *J. Chem. Eng. Data* **1986**, *31*, 37−40.
(39) Cordeiro, J. M. M.; Gomide Freitas, L. C. Study of Water and Dimethylformamide Interaction by Computer Simulation. *Z. Naturforsch. A* **1999**, *54*, 110−116.
(40) Chalaris, M.; Koufou, A.; Samios, J. Molecular Dynamics Simulations of the Liquid Mixtures N,N-Dimethylformamide-Water Using Available Potential Models. *J. Mol. Liq.* **2002**, *101*, 69−79.
(41) Scharlin, P.; Steinby, K.; Domańska, U. Volumetric Properties of Binary Mixtures of N,N-Dimethylformamide with Water or Water-d_2 at Temperatures from 277.13 to 318.15 K. *J. Chem. Thermodyn.* **2002**, *34*, 927−957.
(42) Tomikawa, K.; Kanno, H.; Kimoto, H. A Raman Study of Aqueous DMF and DMA Solutions at Low Temperatures. *Canad. J. Chem.* **2004**, *82*, 1468−1473.
(43) Xu, Z.; Li, H.; Wang, C.; Pan, H.; Han, S. The Methyl C−H Blueshift in N,N-Dimethylformamide-Water Mixtures Probed by Two-Dimensional Fourier-Transform Infrared Spectroscopy. *J. Chem. Phys.* **2006**, *124*, 244502.
(44) Okada, M.; Ibuki, K.; Ueno, M. Temperature Effect on the Reorientational Correlation Time of Water in Formamide− and N,N-Dimethylformamide−Water Mixtures. *Bull. Chem. Soc. Japan* **2012**, *85*, 189−200.
(45) Biswas, S.; Mallik, B. S. Effects of Temperature on the Structure and Dynamics of Aqueous Mixtures of N,N-Dimethylformamide. *J. Chem. Eng. Data.* **2014**, *59*, 3250−3257.
(46) Wang, J.; Gao, W.; Zhong, H.; Liang, C.; Chen, X.; Lüdemann, H.-D.; Chen, L. A Systematic Study on the Intradiffusion and Structure of N,N-Dimethylformamide−Water Mixtures: By Experiment and Molecular Dynamics Simulation. *RSC Adv.* **2016**, *6*, 85603−85611.
(47) Dominguez, H.; Pizio, O. On the Composition Dependence of the Microscopic Structure, Thermodynamic, Dynamic and Dielectric Properties of Water-Dimethyl Formamide Model Mixtures. Molecular Dynamics Simulation Results. *Condens. Matter. Phys.* **2017**, *20*, 43602.
(48) Alam, M. S.; Ashokkumar, B.; Siddiq, A. M. The Density, Dynamic Viscosity and Kinematic Viscosity of Protic and Aprotic Polar Solvent (Pure and Mixed) Systems: An Experimental and Theoretical Insight of Thermophysical Properties. *J. Mol. Liq.* **2019**, *281*, 584−597.
(49) Tomar, D.; Rana, B.; Jena, K. C. The Structure of Water−DMF Binary Mixtures Probed by Linear and Nonlinear Vibrational Spectroscopy. *J. Chem. Phys.* **2020**, *152*, 114707.
(50) Allen, M. P.; Tildesley, D. J. *Computer Simulation of Liquids*; Clarendon Press: Oxford, 1987.
(51) Schoester, P. C.; Zeidler, M. D.; Radnai, T.; Bopp, P. A. Comparison of the Structure of Liquid Amides as Determined by Diffraction Experiments and Molecular Dynamics Simulation. *Z. Naturforsch. A* **1995**, *50*, 38−50.
(52) Gao, J.; Pavelites, J. J.; Habibollazadeh, D. Simulation of Liquid Amides Using a Polarizable Intermolecular Potential Function. *J. Phys. Chem.* **1996**, *100*, 2689−2697.
(53) Chalaris, M.; Samios, J. A Molecular Dynamics Simulation Study of Li^+-Cl^- Ion Pair Dissolved in DMF (−d7). *J. Mol. Liq.* **1998**, *78*, 201−215.
(54) Chalaris, M.; Samios, J. Systematic Molecular Dynamics Studies of Liquid N,N-Dimethylformamide Using Optimized Rigid Force Fields: Investigation of the Thermodynamic, Structural, Transport and Dynamic Properties. *J. Chem. Phys.* **2000**, *112*, 8581−8594.
(55) Vasudevan, V.; Mushrif, H. Field Parameters for N,N-Dimethylformamide (DMF) Revisited: Improved Prediction of Bulk Properties and Complete Miscibility in Water. *J. Mol. Liq.* **2015**, *206*, 338−342.
(56) Jedlovszky, P.; Idrissi, A.; Jancsó, G. Can Existing Models Qualitatively Describe the Mixing Behavior of Acetone with Water? *J. Chem. Phys.* **2009**, *130*, 124516.
(57) Pinke, A.; Jedlovszky, P. Modeling of Mixing Acetone and Water: How Can Their Full Miscibility Be Reproduced in Computer Simulations? *J. Phys. Chem. B* **2012**, *116*, 5977−5984.
(58) Abascal, J. L. F.; Vega, C. A General Purpose Model for the Condensed Phases of Water: TIP4P/2005. *J. Chem. Phys.* **2005**, *123*, 234505.
(59) Pártay, L. B.; Hantal, G.; Jedlovszky, P.; Vincze, Á.; Horvai, G. A New Method for Determining the Interfacial Molecules and Characterizing the Surface Roughness in Computer Simulations. Application to the Liquid−Vapor Interface of Water. *J. Comput. Chem.* **2008**, *29*, 945−956.

https://doi.org/10.1021/acs.jpcb.2c07572
J. Phys. Chem. B 2023, 127, 1050−1062

(60) Jorge, M.; Jedlovszky, P.; Cordeiro, M. N. D. S. A Critical Assessment of Methods for the Intrinsic Analysis of Liquid Interfaces. 1. Surface Site Distributions. *J. Phys. Chem. C* **2010**, *114*, 11169−11179.
(61) Essman, U.; Perera, L.; Berkowitz, M. L.; Darden, T.; Lee, H.; Pedersen, L. G. A Smooth Particle Mesh Ewald Method. *J. Chem. Phys.* **1995**, *103*, 8577−8593.
(62) Abraham, M. J.; Murtola, T.; Schulz, R.; Páll, S.; Smith, J. C.; Hess, B.; Lindahl, E. GROMACS: High Performance Molecular Simulations Through Multi-Level Parallelism from Laptops to Supercomputers. *SoftwareX* **2015**, *1-2*, 19−25.
(63) Nosé, S. A Molecular Dynamics Method for Simulations in the Canonical Ensemble. *Mol. Phys.* **1984**, *52*, 255−268.
(64) Hoover, W. G. Canonical Dynamics: Equilibrium Phase-Space Distributions. *Phys. Rev. A* **1985**, *31*, 1695−1697.
(65) URL: https://github.com/Marcello-Sega/pytim, last accessed: Sept 21, 2022.
(66) Sega, M.; Hantal, G.; Fábián, B.; Jedlovszky, P. PYTIM: A Python Package for the Interfacial Analysis of Molecular Simulations. *J. Comput. Chem.* **2018**, *39*, 2118−2125.
(67) Jedlovszky, P. The Hydrogen Bonding Structure of Water in the Vicinity of Apolar Interfaces: A Computer Simulation Study. *J. Phys.: Condens. Matter* **2004**, *16*, S5389−S5402.
(68) Jedlovszky, P.; Předota, M.; Nezbeda, I. Hydration of Apolar Solutes of Varying Size: A Systematic Study. *Mol. Phys.* **2006**, *104*, 2465−2476.
(69) Pártay, L. B.; Jedlovszky, P.; Vincze, Á.; Horvai, G. Properties of Free Surface of Water-Methanol Mixtures. Analysis of the Truly Interfacial Molecular Layer in Computer Simulation. *J. Phys. Chem. B* **2008**, *112*, 5428−5438.
(70) Pojják, K.; Darvas, M.; Horvai, G.; Jedlovszky, P. Properties of the Liquid-Vapor Interface of Water-Dimethyl Sulfoxide Mixtures. A Molecular Dynamics Simulation and ITIM Analysis Study. *J. Phys. Chem. C* **2010**, *114*, 12207−12220.
(71) Fábián, B.; Jójárt, B.; Horvai, G.; Jedlovszky, P. Properties of the Liquid-Vapor Interface of Acetone-Water Mixtures. A Computer Simulation and ITIM Analysis Study. *J. Phys. Chem. C* **2015**, *119*, 12473−12487.
(72) Horváth, R. A.; Fábián, B.; Idrissi, A.; Szőri, M.; Jedlovszky, P. Investigation of the Liquid−Vapour Interface of Aqueous Methylamine Solutions by Computer Simulation Methods. *J. Mol. Liq.* **2019**, *288*, No. 110978.
(73) Kiss, B.; Fábián, B.; Idrissi, A.; Szőri, M.; Jedlovszky, P. Investigation of the Liquid−Vapor Interface of Water−Formamide Mixtures by Computer Simulation and Intrinsic Surface Analysis. *J. Phys. Chem. C* **2018**, *122*, 19639−19651.
(74) Pártay, L. B.; Jedlovszky, P.; Horvai, G. Structure of the Liquid-Vapor Interface of Water-Acetonitrile Mixtures As Seen from Molecular Dynamics Simulations and Identification of Truly Interfacial Molecules Analysis. *J. Phys. Chem. C* **2009**, *113*, 18173−18183.
(75) Fábián, B.; Szőri, M.; Jedlovszky, P. Floating Patches of HCN at the Surface of Their Aqueous Solutions − Can They Make "HCN World" Plausible? *J. Phys. Chem. C* **2014**, *118*, 21469−21482.
(76) Voronoi, G. F. Recherches sur le Paralléloèders Primitives. *J. Reine Angew. Math.* **1908**, *134*, 198−287.
(77) Okabe, A.; Boots, B.; Sugihara, K.; Chiu, S. N. *Spatial Tessellations: Concepts and Applications of Voronoi Diagrams*; John Wiley: Chichester, 2000.
(78) Medvedev, N. N. *The Voronoi-Delaunay Method in the Structural Investigation of Non-Crystalline Systems*; SB RAS: Novosibirsk, 2000, in Russian.
(79) Kiang, T. Random Fragmentation in Two and Three Dimensions. *Z. Astrophys.* **1966**, *63*, 433−439.
(80) Pineda, E.; Bruna, P.; Crespo, D. Cell Size Distribution in Random Tessellations of Space. *Phys. Rev. E.* **2004**, *70*, No. 066119.
(81) Fábián, B.; Sega, M.; Horvai, G.; Jedlovszky, P. Single Particle Dynamics at the Intrinsic Surface of Various Apolar, Aprotic Dipolar, and Hydrogen Bonding Liquids As Seen from Computer Simulations. *J. Phys. Chem. B.* **2017**, *121*, 5582−5594.
(82) Zaninetti, L. The Voronoi Tessellation Generated from Different Distributions of Seeds. *Phys. Lett. A* **1992**, *165*, 143−147.
(83) Idrissi, A.; Damay, P.; Yukichi, K.; Jedlovszky, P. Self-Association of Urea in Aqueous Solutions: A Voronoi Polyhedron Analysis Study. *J. Chem. Phys.* **2008**, *129*, 164512.
(84) Jedlovszky, P.; Vincze, Á.; Horvai, G. New Insight into the Orientational Order of Water Molecules at the Water/1,2-Dichloroethane Interface: A Monte Carlo Simulation Study. *J. Chem. Phys.* **2002**, *117*, 2271−2280.
(85) Jedlovszky, P.; Vincze, Á.; Horvai, G. Full Description of the Orientational Statistics of Molecules Near to Interfaces. Water at the Interface with CCl_4. *Phys. Chem. Chem. Phys.* **2004**, *6*, 1874−1879.
(86) Geiger, A.; Stillinger, F. H.; Rahman, A. Aspects of the Percolation Process for Hydrogen-Bond Networks in Water. *J. Chem. Phys.* **1979**, *70*, 4185−4193.
(87) Stanley, H. E.; Teixeira, J. Interpretation of the Unusual Behavior of H_2O and D_2O at Low Temperatures. Test of a Percolation Model. *J. Chem. Phys.* **1980**, *73*, 3404−3422.
(88) Darvas, M.; Horvai, G.; Jedlovszky, P. Temperature dependence of the lateral hydrogen bonded clusters of molecules at the free water surface. *J. Mol. Liq.* **2012**, *176*, 33−38.
(89) Sega, M.; Horvai, G.; Jedlovszky, P. Microscopic Origin of the Surface Tension Anomaly of Water. *Langmuir* **2014**, *30*, 2969−2972.
(90) Sega, M.; Horvai, G.; Jedlovszky, P. Two-Dimensional Percolation at the Free Water Surface and its Relation with the Surface Tension Anomaly of Water. *J. Chem. Phys.* **2014**, *141*, No. 054707.
(91) Stauffer, D. *Introduction to Percolation Theory*; Taylor and Francis: London, 1985.
(92) Laage, D.; Hynes, J. T. Do More Strongly Hydrogen-Bonded Water Molecules Reorient More Slowly? *Chem. Phys. Lett.* **2006**, *433*, 80−85.
(93) Vila Verde, A.; Bolhuis, P. G.; Campen, R. K. Statics and Dynamics of Free and Hydrogen Bonded OH Groups at the Air/Water Interface. *J. Phys. Chem. B.* **2012**, *116*, 9467−9481.
(94) Fábián, B.; Senćanski, M. V.; Cvijetić, I. N.; Jedlovszky, P.; Horvai, G. Dynamics of the Water Molecules at the Intrinsic Liquid Surface As Seen from Molecular Dynamics Simulation and Identification of Truly Interfacial Molecules Analysis. *J. Phys. Chem. C* **2016**, *120*, 8578−8588.
(95) Yeh, I. C.; Hummer, G. System-Size Dependence of Diffusion Coefficients and Viscosities from Molecular Dynamics Simulations with Periodic Boundary Conditions. *J. Phys. Chem. C* **2004**, *108*, 15873−15879.
(96) Rideg, N. A.; Darvas, M.; Varga, I.; Jedlovszky, P. Lateral Dynamics of Surfactants at the Free Water Surface: A Computer Simulation Study. *Langmuir* **2012**, *28*, 14944−14953.

https://doi.org/10.1021/acs.jpcb.2c07572
J. Phys. Chem. B 2023, 127, 1050−1062